Available online at www.sciencedirect.com
ScienceDirect
Journal of Power Sources 178 (2008) 309–315
JOURNAL OF POWER SOURCES
www.elsevier.com/locate/jpowsour

Modeling investigation of gradient electrolyte films deposited via convection–diffusion on porous electrode substrates

Liu Junliang, Tian Changan, Kong Xiangrong, Zeng Yanwei *

School of Materials Science and Engineering, Nanjing University of Technology, Nanjing 210009, PR China

Received 10 October 2007; received in revised form 30 November 2007; accepted 30 November 2007
Available online 14 December 2007

Abstract

A numerical simulation based on 1-D upward deposition model has been carried out to investigate the deposition of electrolyte films with gradient microstructures via convection–diffusion process on porous electrode substrates. The simulation results concerning deposition dynamics and structural profiles of the gradient films are in a good agreement with the experimental data. The influences from the solution properties, substrate porosity and evaporation rate of solvent on the microstructural development of deposit layers have been studied by considering the deposition ability and diffusion coefficient of the solute species in porous substrate and the evaporation rate of solvent. It has been found that the concentration distribution in the porous substrate is mainly characterized by a rapid rise up to >10 times its initial value at the deposit–substrate interface and a decaying profile. The uniform deposit layer on the surface of porous substrate and the gradient layer stretching into the substrate are significantly controlled in growth dynamics by the deposition and diffusion abilities of solute for a given evaporation rate of solvent. Moreover, the solute's deposition ability appears to pose more influence on the thickening of top-deposit layer while the diffusion coefficient of solute is the main factor to control the depth development of the gradient layer inside the substrate.

Keywords: Convection–diffusion; Electrolyte films; Gradient microstructure; Porous electrodes; SOFCs

1. Introduction

It is well known that developing the intermediate and low temperature solid oxide fuel cells (SOFCs) has been faced with two new challenges: drastic drop in ionic conductivity of cell's materials and remarkable increase of interfacial polarization resistances between cathode/anode and electrolyte layers as the operation temperature goes down. To conquer these problems, two basic strategies have been adopted: (1) seeking novel materials with high ionic conductivity at intermediate and low temperatures and (2) exploring novel microstructures of cell components by using novel fabrication and processing techniques, such as fabricating supported electrolyte films, developing composite cathodes/anodes with uniform or gradient microstructures, etc., to reduce the interfacial polarization resistances between cathode/anode and electrolyte layers [1–6].

It has been recognized that the oxygen ionic flux can be increased several folds when an YSZ electrolyte membrane was thinned from few hundreds to few tens micros at 800 °C. Such an electrolyte film may be built upon the porous cathodes or anodes via vapor phase deposition (VD), electrochemical and vapor phase electrolytic deposition (ECVD and VED), sol–gel coating techniques, as well as slurry or colloidal deposition, etc. [7–13]. What is more notable is that the concept of functionally graded materials (FGM) has been introduced recently to the fabrication of SOFCs components to improve their interfacial conditions and electrochemical performance. Some single-phase cathode materials (e.g. LSM/LSC) and composite cathodes (e.g. LSM/LSC–YSZ/GDC) were prepared on YSZ electrolytes via different methods such as screen printing, slurry-spraying, spray-painting, and slurry-coating, resulting in the reduced interfacial polarization resistances and improved electrochemical performances [14–18]. Nonetheless, the works reported in the literature were mostly concerned with electrolyte-supported porous cathodes or anodes with compositional gradients. This kind of structures is usually of a large thickness of electrolytes

* Corresponding author. Tel.: +86 25 83587254; fax: +86 25 83588316.
E-mail address: zengyanwei@tom.com (Y. Zeng).

0378-7753/$ – see front matter © 2007 Elsevier B.V. All rights reserved.
doi:10.1016/j.jpowsour.2007.11.111

and, therefore, unfavorable for the intermediate temperature SOFCs.

Recently, our group has successfully fabricated electrode-supported electrolyte thin films with gradient microstructure by taking advantage of the convection–diffusion effect of solution in porous solid media [19]. The as-prepared YSZ-film/substrate structures are characterized by a dense YSZ film of ~10 μm on the surface of substrate, a uniform filling layer of ~50 μm just beneath the interface between the dense film and the substrate, and then a diffuse layer stretching as deep as ~250 μm in to the micro-pores of the substrate. The electrolyte/electrode interface structures of this kind are expected to greatly reduce the interfacial polarization resistance and favor the enhancement of electrode electrochemical reactions for both single-phase mixed conductive cathodes and composite cathodes [20]. The film-depositing method based on the convection–diffusion effect is simple, controllable, economical and potentially applicable to fabricating electrode-supported gradient electrolyte films for SOFCs.

In order to reach a better understanding of the formation details of deposit films with gradient microstructure on the porous electrode via convection–diffusion route, a numerical simulation of film deposition has been performed with a 1-D convection–diffusion model in this paper. The influences from the evaporation rate of solvent and the properties of solutions on the formation and microstructures of deposit films were studied with the consequences in a good agreement with the experimental results, which may serve as a guide to further improving the electrochemical and mechanical compatibilities between electrolyte and electrode materials of SOFCs.

2. Phenomenological model for simulation

2.1. Film deposition via convection–diffusion

The convection–diffusion process that was utilized to fabricate electrolyte films with gradient structure on porous substrates may be outlined as follows. As schematically shown in Fig. 1, a pre-sintered porous substrate is mounted on a well-designed glass vessel with its peripheral edge tightly sealed and properly kept in contact with the solution containing volatile solvent (e.g. methanol) and chemical species for film composition as solutes. Under the hydraulic pressure of liquid and capillary force, the solution may penetrate into the porous substrate and flow upward as convection. When the solution comes out at top surface of the substrate, the solvent evaporation occurs, leaving the solute species at the surface and resulting in a higher concentration of species in the surface area than elsewhere in the system, which in turn provokes a diffusion of the species in the direction opposite to the convection. As the solvent evaporation proceeds, regardless of the downward diffusion, a higher and higher concentration of solute will be established at the surface due to the continuous upward convection of solution and, as a result, the solute species begins to precipitate and deposits on the surface of the substrate when the concentration reaches its saturation value. Obviously, such a continuous convection–diffusion process will finally lead to the formation of a deposit layer at the surface of substrate and a downward diffusing concentration profile inside the porous substrate with its peak beneath the deposit layer.

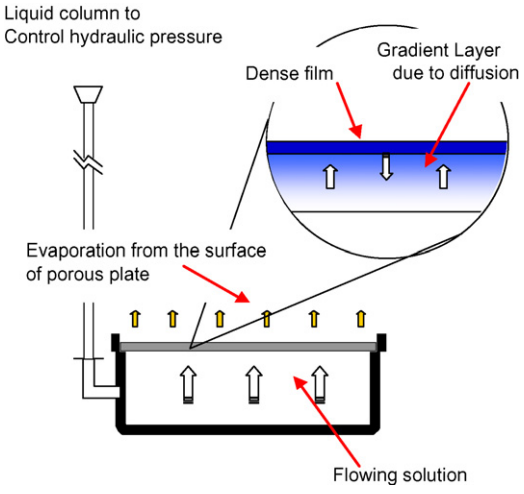

Fig. 1. The schematic of lab setup for fabricating supported electrolyte film with gradient porous structure.

2.2. Upward deposition model and mathematic equations

In order to effectively carry out the modeling study, a phenomenological upward deposition model is presented on the convection–diffusion process with which the deposition of solute species is confined to top surface of the substrate while the downward diffusing concentration profile inside the porous substrate will finally contribute to the formation of gradient layer, as the stretching part of top deposit layer. Besides, for the sake of simplicity, it is assumed that the substrate is uniform in the pore structure and its radial size is so large that the influences from its peripheral boundary can be neglected. Therefore, the convection–diffusion process in a porous substrate happens only along the direction perpendicular to its surface and the following one-dimensional partial differential equation can be used for the simulation:

$$\frac{\partial c_{\mathrm{slu}}}{\partial t} = D\frac{\partial^2 c_{\mathrm{slu}}}{\partial z^2} - u_{\mathrm{s}}\frac{\partial c_{\mathrm{slu}}}{\partial z}, \quad (t > 0, 0 \le z \le d) \tag{1}$$

where c_{slu} refers to the concentration of solute, D to its diffusion coefficient in the given solution, u_{s} to the convection velocity of solution and d is the thickness of substrate.

As the initial and boundary conditions for Eq. (1), the following equations were adopted since the concentration of solute in the substrate is the same everywhere at the beginning of solvent evaporation and the bottom of substrate is always kept in contact with the solution, whose volume is so large that the concentration change can be neglected during the film deposition:

$$\begin{aligned} c_{\mathrm{slu}}(z, 0) &= c_0 \\ c_{\mathrm{slu}}(0, t) &= c_0 \end{aligned} \tag{2}$$

Now let us consider the details of solvent evaporation, solute's deposition and downward diffusion, thickening and densifica-

tion of deposit layer that are happening simultaneously with the upward convection of solution.

2.2.1. Solvent evaporation

Since the liquid surface is always controlled at the same level with that of deposit layer during all the experiment of film deposition, it is believed that the realistic evaporation rate of solvent per unit surface area of substrate (mg cm^{-2} s) should be proportional to the porosity of deposit layer and, consequently, its mathematic expression can be simply written as:

$$V = K_1\phi \tag{3}$$

where ϕ *is* the porosity of deposit layer and K_1 is the proportional coefficient, which takes into account all the other influences on the solvent evaporation.

It is clearly evident that the porosity ϕ should assume the value for the substrate at the beginning of evaporation because the deposit layer is not yet formed at that time. Obviously, the proportional coefficient K_1, depending on the given experimental conditions, can be evaluated by using the experimental data of V and ϕ from the substrate.

On the other hand, with respect to the mass conservation, the solvent evaporation rate at any time should also be equal to the quantity of solvent flowing across the deposit–substrate interface:

$$V = c_{\mathrm{slv}}(d, t)u_{\mathrm{s}}(d, t) \tag{4}$$

where c_{slv} is the concentration of solvent and u_{s} is the convection velocity of solution. It should be noted that the convection velocity of solution may differ from place to place across the whole thickness of substrate due to the concentration variation of solute. In the simulation study, the following relation was used to make correction to the value of u_{s}:

$$V_0 = n_{\mathrm{slv}}\overline{V_{\mathrm{slv}}} + n_{\mathrm{slu}}\overline{V_{\mathrm{slu}}} \tag{5}$$

where n_{slv} and n_{slu} are the molar concentrations of solvent and solute, respectively, and $\overline{V_{\mathrm{slv}}}$ and $\overline{V_{\mathrm{slu}}}$ are their partial molar volumes and can be experimentally determined.

2.2.2. Deposition and deposition factor

To describe the partition of the solute left after the evaporation of solvent, a parameter called deposition factor, η, is defined as the ratio of the deposit mass to the total solute mass that is carried up to the deposit–substrate interface by solvent. Therefore, the deposition part Δm_{de} and the diffusion part Δm_{di} at any time interval Δt can be written as:

$$\Delta m_{\mathrm{de}} = \eta\Delta m_{\mathrm{t}}, \quad \Delta m_{\mathrm{di}} = (1-\eta)\Delta m_{\mathrm{t}}, \quad \text{and} \quad \eta = \frac{\Delta m_{\mathrm{de}}}{\Delta m_{\mathrm{t}}} \tag{6}$$

Obviously, the deposition factor is proportional to the deposit part, which should be closely associated with the solute concentration in the deposit layer. With reference to the knowledge about the coarsening of precipitate particles, when the process is controlled by diffusion the volumetric increment ΔV at a time interval Δt is:

$$\Delta V \propto \frac{8D\sigma vc(\infty)}{9k_{\mathrm{B}}T}\Delta t \tag{7}$$

where $c(\infty)$ is the bulk concentration of solute in the solution. Also, according to the JMA theory for phase transformation, the conversion fraction of mother phase to new phase ζ for a system with incipient nucleation only is determined by the formula below:

$$\zeta = 1 - \exp\left(-\frac{4\pi N_0(u\Delta t)^3}{3}\right) \tag{8}$$

where $(u\Delta t)$ denotes the growth length in each dimension at a time interval, Δt [21]. Therefore, the term $(u\Delta t)^3$ in Eq. (8) should be equivalent to the ΔV in Eq. (7) and, as a consequence, the deposition factor could be expressed by:

$$\eta = \frac{\Delta m_{\mathrm{de}}}{\Delta m_{\mathrm{t}}} = 1 - \exp[-K_2 c_{\mathrm{slu}}(d, t)] \tag{9}$$

where K_2 is a parameter related to the depositing ability of solute from the solution.

2.2.3. Downward diffusion of solute

As is aforementioned, apart from the depositing part, the other part of the solute carried up to the deposit–substrate interface by convection is to diffuse downwards due to the driving of concentration gradient, leading to the change in solute concentration profile. It is clearly evident that the total variation of solute concentration profile should come from two contributions, one from the diffusion part Δm_{di} of the solute at the interface, which may be simply described by a Gaussian distribution:

$$\Delta c_{\mathrm{slu}} = \frac{\Delta m_{\mathrm{di}}}{\sqrt{\pi D\Delta t}}\exp\left\{-\frac{(d-x)^2}{4D\Delta T}\right\} \tag{10}$$

the other one is from the re-distribution of the concentration of solute in substrate at a previous moment. Obviously, the latter contribution will not cause any change in the total quantity of solute inside the substrate.

2.2.4. Thickening and densification of deposit layer

As the solute in the deposit layer precipitates out, the thickening and densification of deposit layer will happen at the same time and, therefore, the following general equation should be considered:

$$\rho_0\left(-\frac{\mathrm{d}\phi}{\mathrm{d}t}\right)\delta + \rho_0(1-\phi)\frac{\mathrm{d}\delta}{\mathrm{d}t} = \frac{\mathrm{d}m_{\mathrm{de}}}{\mathrm{d}t} \tag{11}$$

where ρ_0 and δ are the mass density of precipitated phase and the apparent thickness of the deposit layer, respectively.

2.2.5. Mass conversation condition

In the present simulation study, the total mass of solute that was carried up to the interface was determined by:

$$\Delta m_t = \int_{d-u_{\mathrm{s}}\Delta t}^{\mathrm{d}} c_{\mathrm{slu}}(z, t)\,\mathrm{d}z \tag{12}$$

while the mass of solute that was transported into the substrate through the bottom surface can be given by:

$$\Delta m_{\text{in}} = c_0 u_S(0, t)\Delta t \tag{13}$$

Obviously, the input mass of solute should be equal to the sum of the mass increment of solute within the substrate and the deposit mass in the given time interval. So, one has the following mass conversation relation:

$$\Delta m_{\text{in}} = \int_0^{\text{d}} \Delta c_{\text{slu}} \text{d}z + m_{\text{de}} \tag{14}$$

which was used to check the reliability of simulating calculation at each iteration step and to correct any possible calculation errors.

2.3. Numerical simulations

The numerical simulation was carried out in a procedure as illustrated in Fig. 2. It started with the data input and evaluation of initial and boundary conditions, evaporation rate curves, and the related parameters including diffusion coefficient, thickness and porosity of substrate, etc., as listed in Table 1. For any time point, the concentration distribution and the thickness of uniform deposit layer were obtained through the iterative solving operations of the discretized 1-D differential equations for convection–diffusion process and the thickening and densification of deposit layer. The relative calculation error boundary was set at 10^{-3} and the calculation stopped when the set deposition time was fully covered.

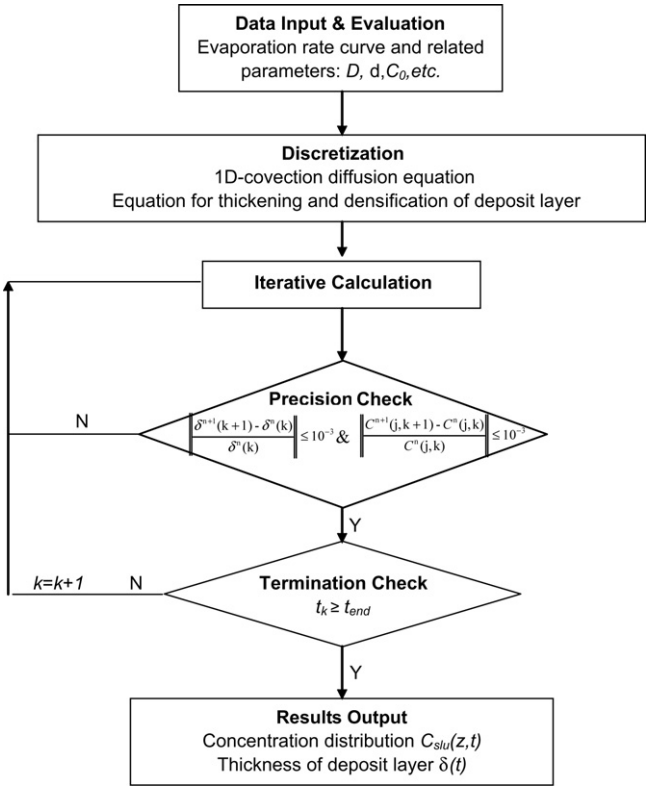

Fig. 2. The flow chart of the numerical simulation.

Table 1
Related parameters for numerical simulation and the fitting parameters for evaporation rate curves

Parameters	Values
Thickness of substrate, d	2.0 mm
Porosity of substrate, φ_0	0.40 ± 0.01
Density of fresh deposit, ρ_0	1.91 g cm^{-3}
Initial concentration of solute c_0	0.2 mol L^{-1}
Partial molar volume of CH_3OH: $\overline{V_{\text{slv}}}$	40.04 cm^3 mol^{-1}
Partial molar volume of $ZrOCl_2 \cdot 8H_2O$: $\overline{V_{\text{slu}}}$	13.42 cm^3 mol^{-1}
a, b, c for evaporation rate curve 1	0.0431, 0.1078,0.6667
a, b, c from best-fit to evaporation rate curve 2	0.0399, 0.0998, 0.3333; $R^2 = 0.9813$
a, b, c for evaporation rate curve 3	0.0255, 0.0638, 0.0667
a, b, c for evaporation rate curve 4	0.0144, 0.0360, 0.0050

3. Results and discussion

3.1. Different deposition modes based on an experimental case

It should be pointed out that the present simulation study was carried out with a starting point based on our experimental research for the fabrication of electrolyte films with gradient structure via convection–diffusion route on porous substrates. The solution system was composed of methanol as solvent and zirconium chloride plus yttrium chloride in a stoichiometry of 8 mol%Y_2O_3–ZrO_2 (YSZ) as solute with a concentration of 0.2 M. The substrate was a porous well-sintered alumina plate with 30 mm in diameter, 1.5 mm in thickness and a porosity of $40 \pm 1\%$.

In order to reveal how the film deposition via the convection–diffusion process is influenced by the deposition conditions, four different evaporation rate curves, as shown in Fig. 3, have been used in the present simulation study, in which curve 2 was a best-fit to the experimental data from the aforementioned system, while the curves 1, 3 and 4 were derived out of the curve 1 by evaluating the parameters with different values, as listed in Table 1, by using the following exponential decay

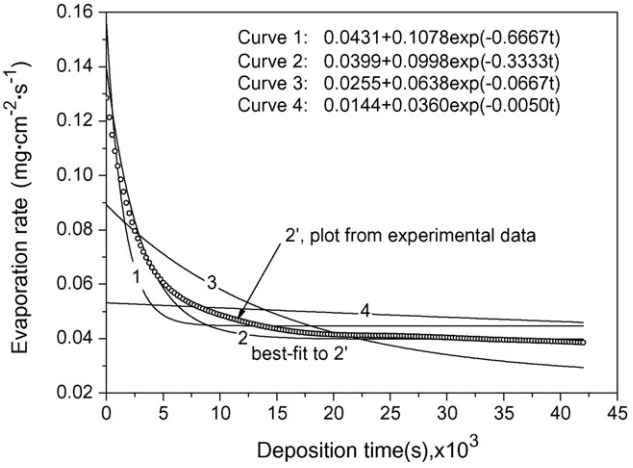

Fig. 3. Evaporation rate versus deposition time.

function:

$$V = a + b\ \exp[-ct] \tag{15}$$

where a, b and c are the characteristic parameters of film deposition modes. The parameter a can be understood as a residual evaporation rate and b as the maximum reducible evaporation rate, whose magnitudes might be determined by some mechanism of deposit layer on porous substrates. Clearly, $a+b$ represent the initial evaporation rate of solvent, simply determined by the porosity of substrate. The parameter c appears to be closely associated with the formation dynamics and structural details of deposit layer. When the parameter c is increased, the evaporation rate V will be decreased at a higher velocity, suggesting a fast deposition and densification dynamics. Therefore, as their characteristic parameters are evaluated with the values indicated in Table 1, the four different evaporation rate curves denoted by curve 1, curve 2, curve 3 and curve 4 are actually corresponding to four different deposition modes, respectively, from fast to slow densifications.

3.2. Deposition profiles for uniform and gradient layers

Starting from the experimental evaporation rate curve 2, where the characteristic parameters $K_2 = 0.09$ and $D = 8.0 \times 10^{-7}\ \mathrm{cm^2\ s^{-1}}$, the concentration distributions in the porous substrate, deposition factor, thickness of fresh deposit layer as well as the equivalent thickness to the sintered dense ZrO_2 layer were calculated as a function of deposition time and plotted in Figs. 4–6.

It can be seen from Fig. 4 that as the deposition time increases, the concentration at the surface of substrate shows a rapid rise, especially in the initial stage and, finally, up to as high as 12 c_0. In practice, when the concentration arrives at a value higher than the saturation point of $ZrOCl_2{\cdot}8H_2O$ in CH_3OH, the film's deposition may be quickly provoked. As to the concentration distribution along the thickness of substrate, a monotonous and fast decaying profile can be seen and commonly characterized by a gradual decrease to a value close to c_0 in a depth. It is clear that a rapid rise of solute concentration at the surface of substrate is due to the convection of solution and fast evaporation of solvent, while the downward diffusion of solute should be responsible for the decaying concentration profiles.

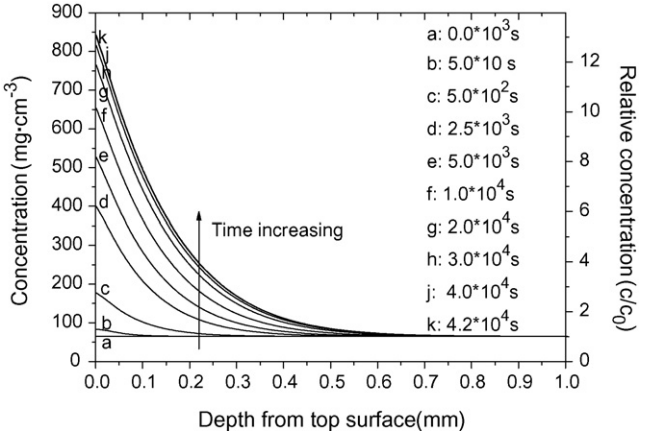

Fig. 4. The concentration distributions as a function of deposition time ($K_2 = 0.09$, $D = 8.0 \times 10^{-7}\ \mathrm{cm^2\ s^{-1}}$).

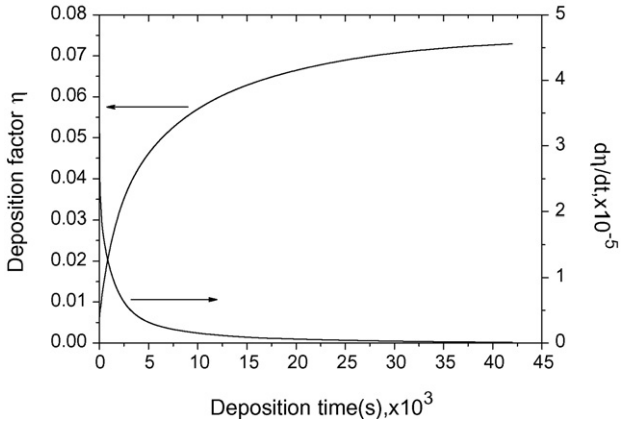

Fig. 5. Deposition factor and its differential as a function of deposition time.

As shown in Fig. 5, the deposition factor increases rapidly in the initial stage and then gradually grows to a stable value in the middle and later stages. It suggests that in the initial stage, the flow resistance is small and the accumulation of solute at the surface is increased rapidly, while in the subsequent stages the flow resistance appears to be remarkably increased, leading to a slowly decelerating deposition process. Besides, it is interesting to note that the magnitude of deposition factor in the whole span of deposition time is lower than 0.075. Such a small deposition factor strongly suggests that most of the solute carried up to the deposit–substrate interface by convection is brought back into the porous substrate by diffusion and, therefore, the formation of the deposit layer is actually carried out slowly. Fig. 6 illustrates the thickening behavior of the deposit layer with the increasing deposition time. It can be seen that the thickening rate of the deposit layer appears to speed up from the beginning through the following 3 h, in response to the remarkably increasing deposition factor, and then it keeps a constant pace, suggesting a stable thickening process in the later period of deposition time.

According to the simulation results shown in Fig. 4, the gradient layer after a deposition time of 12 h is estimated at about 420 μm in thickness when the truncation point is set at

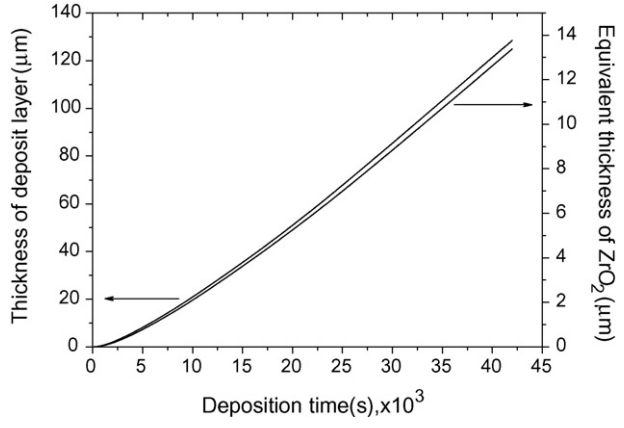

Fig. 6. Thickness of deposit layer as a function of deposition time.

a depth where the local concentration is 1.05 times the initial concentration. Likewise, from Fig. 6, the fresh deposit layer shows an equivalent sintered ZrO_2 thickness of 13.38 μm. These results are in a good agreement with the experimental data: about 300 μm for the gradient layer and about 12 μm for the dense top layer [19].

3.3. Porosity variation and thickening behavior of deposit layers

As an important microstructural parameter, the porosity variation of top deposit layer is directly related to the evaporation rate change by Eq. (3) according to the upward deposition model. Therefore, the porosity–deposition time curve for each case has been derived from its own evaporation rate curve, as shown in Fig. 3, and presented in Fig. 7, which clearly shows a porosity–reduction dynamics for the top deposit layer from its initial value determined by substrate.

Now let us turn to the thickening behavior of deposit layers in the convection–diffusion process. In order to investigate the influences of the properties of solution, porous substrates and other evaporation conditions on the thickness of top deposit layer and the following gradient layer, the parameters K_2 for deposition factor and diffusion coefficient D have been adjusted to simulate different modes from fast to slow densifications through the deposition factor equation and evaporation rate curves. The simulation results were presented in Figs. 8–11.

As shown in Figs. 8 and 9, with $D = 8.0 \times 10^{-7}\ \mathrm{cm^2\ s^{-1}}$, the thickness of the top deposit layer is remarkably increased for each evaporation case as K_2 increases from 0 to 1 and then gradually up to a certain value with the further increasing of K_2, while the final depths of gradient layers show fast decrease as a function of K_2, especially when K_2 increases from 0 to 1.

In view of the fact that the magnitude of K_2 actually reflects the deposit ability of solute from solution, the solute is difficult to deposit from the solution when K_2 is of small value. Obviously, this will lead to a great concentration gradient to drive more solute to diffuse back to the substrate. Therefore, it is believed that a thinner deposit layer on the surface of substrate is necessarily accompanied by a deeper gradient layer inside the substrate.

On the other hand, when K_2 is increased, the solute is expected to be more capable of depositing and a fast thickening

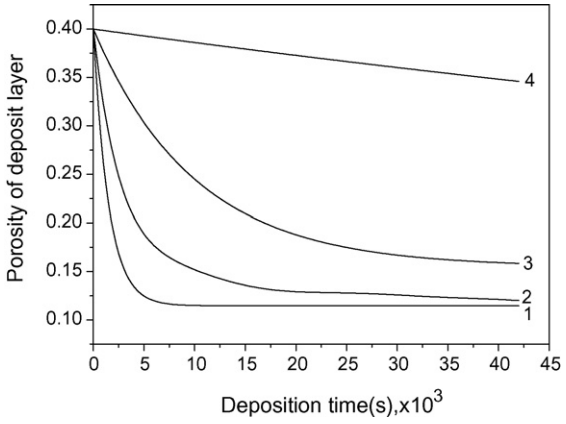

Fig. 7. The porosity of deposit layer as a function of deposit time (the number beside each curve is corresponding to the one of evaporation rate curve, from 1 to 4.).

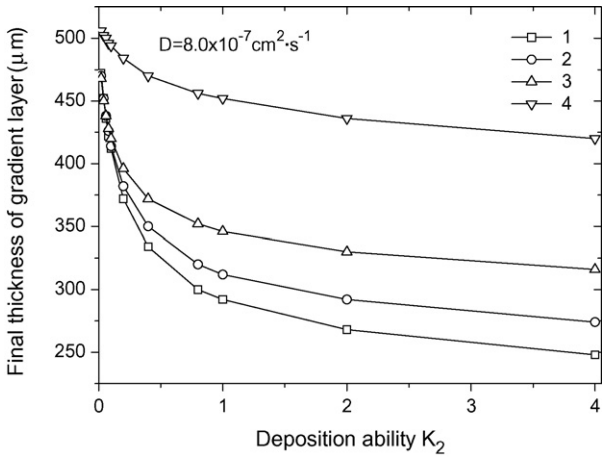

Fig. 8. The final thickness of gradient layer as a function of K_2 for different evaporation rates from 1 to 4.

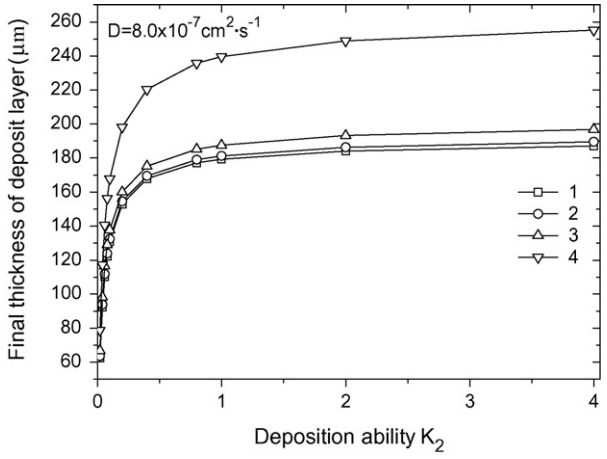

Fig. 9. The final thickness of top deposit layer as a function of K_2 for different evaporation rates from 1 to 4.

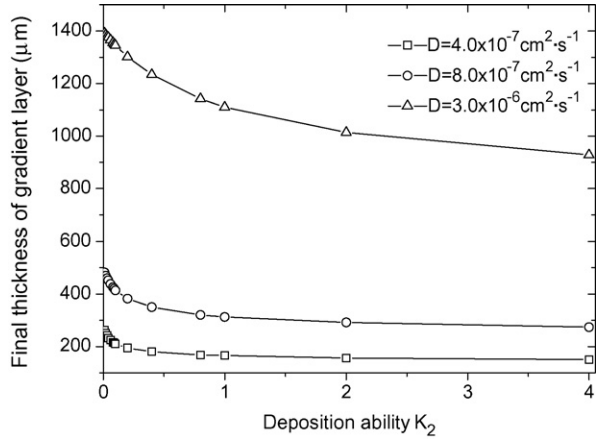

Fig. 10. The final thickness of gradient layer as a function of K_2 for different diffusion coefficients with the evaporation rate curve 2.

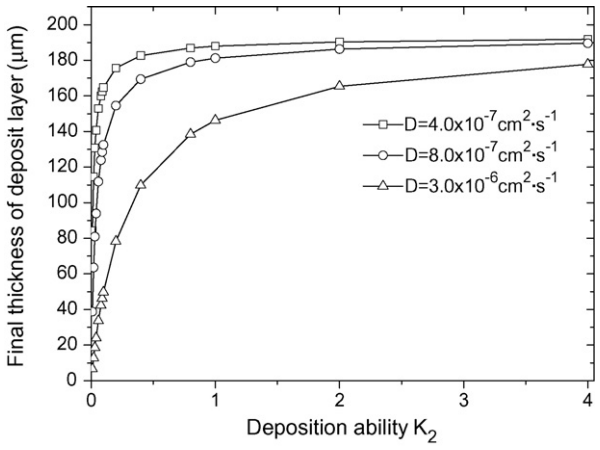

Fig. 11. The final thickness of deposit layer as a function of K_2 for different diffusion coefficients with the evaporation rate curve 2.

of top deposit layer may take place. In this case, the concentration and its gradient at the deposit–substrate interface should be relatively low and it makes gradient layers with a decreased depth. As K_2 increases further, the concentration may be rapidly reduced due to large deposit factor and, as a result, the changing rates of the depth of gradient layer and the thicknesses of top deposit layer are both attenuated remarkably.

As to the influences from different evaporation rate curves, the slow densification gives a relatively low flow resistance and the solvent evaporation may have a high rate for a long time. Thus the amount of accumulated solute at the surface should become large regardless of a slow increase in the local concentration. As a result, the thickness and depth of deposit layers could be larger in the slow densification modes than those in the fast modes.

As illustrated in Figs. 10 and 11, where the thickness–K_2 relationship curves were worked out based on the evaporation rate curve 2 and with different values for the diffusion coefficient D, it can be seen that more solute at the surface may diffuse back into the substrate to form a deeper diffusion front as the diffusion coefficient is increased. In this case, the thickening of top deposit layer proceeds only at a lower speed. Clearly, a large diffusion coefficient favors the formation of deeper diffusion profiles and a slow thickening of top deposit layers.

4. Conclusions

In this paper, the deposition of electrolyte films with gradient microstructure via convection–diffusion process on a porous substrate has been investigated by a numerical simulation based on the experimental data. The simulation results are in a good agreement with the experimental data and have clearly revealed the deposition dynamic details of deposit layers on the surface of substrate and into its porous structure. From this simulation study, the following main conclusions may be drawn out:

(1) The exponential equation, $V = a + b\exp[-ct]$, can be effectively used to fit the experimental data of solvent evaporation rate. It may be further used to explore the growth mechanism of deposit layer according to the physical meaning of the parameters contained in it.
(2) The concentration distribution in the porous substrate is characterized by a rapid rise at the deposit–substrate interface as the deposition time increases due to the solution convection and solvent evaporation, which is followed by a decaying profile due to the downward diffusion of solute.
(3) As the deposition time increases, the deposition factor increases very rapidly in the initial stage, and gradually becomes constant in the later stage. The relatively small magnitude of deposition factor, <0.075, during the whole deposition process reveals that most of the solute carried up to the deposit–substrate interface due to the convection is brought back in to the substrate.
(4) The deposition dynamics of solute is closely associated with its deposition ability and diffusion ability, as well as the evaporation rate of solvent. The deposition ability, K_2, appears to pose more influence on the thickening of top deposit layer while the diffusion coefficient D of solute is the main factor to control the depth development of the gradient layer inside the substrate.
(5) For a given evaporation rate, an enlarged deposition factor leads to a rapid rise in the thickness of top deposit layer while a larger diffusion coefficient will allow the gradient deposit layer to stretch deeper.

References

[1] S. Park, J.M. Vohs, R.J. Gorte, Nature 404 (2000) 265–267.
[2] G. Schiller, et al., Proceedings of the 4th European SOFCs Forum, vol. 37, 2000.
[3] B.C.H. Steele, Solid State Ionics 129 (2000) 95–110.
[4] S. de Souza, S.J. Visco, L.C. Dejonghe, J. Electrochem. Soc. 144 (1997) L35.
[5] S.C. Singhal, Solid State Ionics 152 (2002) 405–410.
[6] T. Suzuki, I. Kosacki, H.U. Anderson, Solid State Ionics 151 (2002) 111–121.
[7] Y. Akiyama, N. Imaishi, Y.S. Shin, S.C. Jung, J. Cryst. Growth 241 (2002) 352–362.
[8] G. Di Giuseppe, J.R. Selman, J. Mater. Res. 16 (2001) 2983–2991.
[9] Y. Uchimoto, K. Tsutsumi, T. Ioroi, Z. Ogumi, J. Am. Ceram. Soc. 83 (2000) 77–81.
[10] T.W. Kueper, S.J. Visco, L.C. De Jonghe, Solid State Ionics 52 (1992) 251–259.
[11] M. Stech, P. Reynders, J. Rodel, J. Am. Ceram. Soc. 83 (2000) 1889–1896.
[12] J. Will, H.K.M. Hruschka, L. Gubler, L.J. Gauckler, J. Am. Ceram. Soc. 84 (2001) 328–332.
[13] L.C. De Jonghe, C.P. Jacobson, S.J. Visco, Annu. Rev. Mater. Res. 33 (2003) 169–182.
[14] D. Herbstritt, et al., J. Electrochem. Soc. 146 (1999) 972.
[15] N.T. Hart, N.P. Brandon, M.J. Day, J.E. Shemilt, J. Mater. Sci. 36 (2001) 1077–1085.
[16] N.T. Hart, N.P. Brandon, M.J. Day, N. Lapena-Rey, J. Power Sources 106 (2002) 42–50.
[17] P. Holtappels, C. Bagger, J. Eur. Ceram. Soc. 22 (2002) 41–48.
[18] C. Xia, W. Rauch, W. Wellborn, M. Liu, Electrochem. Solid State Lett. 5 (2002) A217–A220.
[19] Y. Zeng, C. Tian, J. Liu, J. Mater. Sci. 42 (2007) 2387–2392.
[20] Z. Yanwei, T. Changan, B. Limei, J. Power Sources 139 (2005) 35–43.
[21] D. Feng, C. Shi, Z. Liu, Introduction to Materials Science–An Integrated Approach, Chemical Industry Publishing Co. Ltd. (Beijing), 2002, pp. 568–572.